

PROCEEDINGS OF SPIE

[SPIDigitalLibrary.org/conference-proceedings-of-spie](https://spiedigitallibrary.org/conference-proceedings-of-spie)

Coupled membrane free optical microphone and optical coherence tomography keyhole measurements to setup welding laser parameters

Authier, Nicolas, Touzet, Enzo, Lücking, Fabian, Sommerhuber, Ryan, Bruyère, Vincent, et al.

Nicolas Authier, Enzo Touzet, Fabian Lücking, Ryan Sommerhuber, Vincent Bruyère, Patrick Namy, "Coupled membrane free optical microphone and optical coherence tomography keyhole measurements to setup welding laser parameters," Proc. SPIE 11273, High-Power Laser Materials Processing: Applications, Diagnostics, and Systems IX, 1127308 (2 March 2020); doi: 10.1117/12.2543999

SPIE.

Event: SPIE LASE, 2020, San Francisco, California, United States

Coupled Membrane-free Optical Microphone and Optical Coherence Tomography keyhole measurements to setup welding laser parameters

Nicolas Authier^a, Enzo Touzet^a, Fabian Lücking^b, Ryan Sommerhuber^b, Vincent Bruyère^c, and Patrick Namy^c

^aCommissariat à l’Energie Atomique et aux Energies Alternatives, 21120 Is-sur-Tille, France

^bXarion Laser Acoustics GmbH, Ghegastrasse 3, 1030 Vienna, Austria

^cSIMTEC, 155, Cours Berriat, 38000 Grenoble, France

ABSTRACT

The measurement of depth of a laser capillary in industrial conditions by Optical Coherence Tomography technique is demonstrated in this work. This paper highlights the results achieved by the recent combination of ultrasound sensitive membrane-free optical microphone by XARION and PRECITEC’s OCT IDM system. Joint interpretation of the ultrasound spectrograms and the digging curves of the keyholes enables better understanding of the dynamics of the melted metal and determination of the ideal welding parameters.

Keywords: Laser spot welding, airborne acoustic emissions, membrane-free optical microphone, optical coherence tomography, capillary depth measurements, inline welding process control.

1. INTRODUCTION

New mature technologies have emerged on the market for laser welding inline control purposes.¹ Among all these technical advances, one of the most remarkable is in particular that concerning the measurement of the depth of the vapor capillary (keyhole) by Optical Coherence Tomography (OCT).^{2,3} By nature, this measurement is only possible if a sufficiently deep capillary is formed. Below a limit depending on the material and the power density, as for instance in the welding mode called ”conduction limited”, this measurement technique fails. The purpose of this article is to highlight the results achieved by the recent combination of the ultrasound sensitive membrane-free optical microphone⁴ by XARION and PRECITEC’s OCT In-process Depth Meter (IDM) system. We show that the acoustic emissions of the laser welding pulses extend far beyond the audible spectrum, with an especially rich frequency range between 40 and 600 kHz. Joint interpretation of the spectrograms and the digging curves of the keyholes enables better understanding of the dynamics of the melted metal and determination of the ideal welding parameters., in particular adjustment of the temporal modulation of the laser source power (power pulse shaping).

2. IN-LINE SYSTEMS

2.1 Optical Coherence Tomography for welding

The system is composed of three major components that form a surprisingly simple to setup Michelson-instrumented welding laser head:

- An electronic unit (Figure 1 left - items 1-4) that delivers the light of a Superluminescent Laser Diode (SLD) and in return analyses the interference pattern and deduces the keyhole depth,
- An instrumented welding head that embeds the IDM light collimating module and the interferometer reference box (items 8-17),

Further author information: (Send correspondence to Nicolas Authier)

Nicolas Authier: E-mail: nicolas.authier@cea.fr, Telephone: 33 3 80 23 51 60

High-Power Laser Materials Processing: Applications, Diagnostics, and Systems IX, edited by Stefan Kaierte, Stefan W. Heinemann, Proc. of SPIE Vol. 11273, 1127308 · © 2020 SPIE
CCC code: 0277-786X/20/\$21 · doi: 10.1117/12.2543999

- A remote standard PC that runs a driver for control (items 21-22) and data saving.

The light of the SLD with broad spectrum (gaussian-shaped centred at 1550 nm with 40 nm FWHM) is injected co-axially into the welding laser beam and is reflected by the bottom of the keyhole (Figure 1 - item 19). At the beam splitter (item 9), the addition of the back-scattered field of the reference arm (item 10-11) and the one of the sample arm gives rise to an interference pattern transported back by the IDM fiber (item 7) to the electronic unit which is decoded using a spectrometer and a linear CCD (item 4). An ultra-fast inverse Fourier transform gives the depth of the depression of the surface at a maximum sampling rate of 70 kHz.

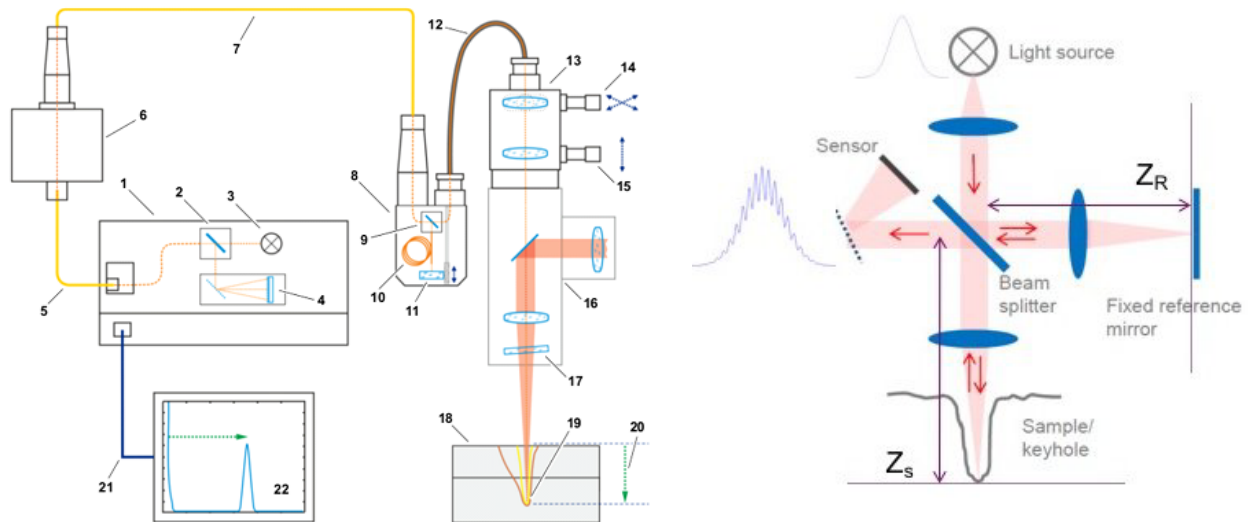


Figure 1. Left: Electronic unit and IDM equipped laser head (PRECITEC IDM manual). Right: IDM Michelson principle.

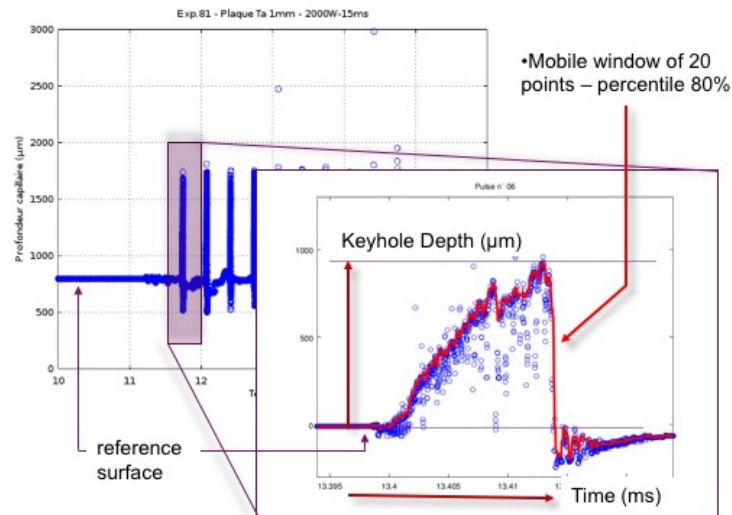


Figure 2. IDM signal of a 10 pulses bead recorded at 70 kHz and zooming in one of them. Laser source: TRUMPF HL506P. Laser pulse duration: 15 ms.

Figure 2 shows a recording of a short 10-laser pulses weld, in which it can be seen that all single measurements (blue circles) form a cloud of points where the statistical depth (red curve) has to be evaluated. Even if, from a

theoretical point of view, the axial resolution is approximately $0.44 \lambda_0^2 / \Delta\lambda$ which is about $30 \mu\text{m}$ in this case, the reflection can occur:

- on the root of the keyhole in a single reflection event (the expected measurement),
- on the root of the keyhole after multiple reflections, which leads to an overestimation of the depth,
- on fold of the liquid metal wall of the keyhole or on metallic spatters ejected from it, which leads to underestimation of the depth.

Thus signal points collected by the IDM are true optical path length measurements, where the corresponding location of the reflection in the keyhole is unknown. This implies that the evaluated depth is not a measurement anymore but more an estimation subjected to the right adequacy between filter type and application. For our experiments, the statistical filter used on the signal is a percentile calculation in a moveable window frame. The optimal adjustment of the parameters (percentile and number of points for the window size) is done by comparison to bead cross-sections. Doing so, this calibration phase smooths the slight difference between keyhole depth (theoretical OCT measurement) and fused depth (cross sections).

2.2 Membrane-free Optical Microphone

The optical microphone works on the principle of interferometry and consists of a control unit containing a laser which sends its light over an optical fiber to a sensor head. This sensor head consists of a pair of parallel, semi reflective mirrors.

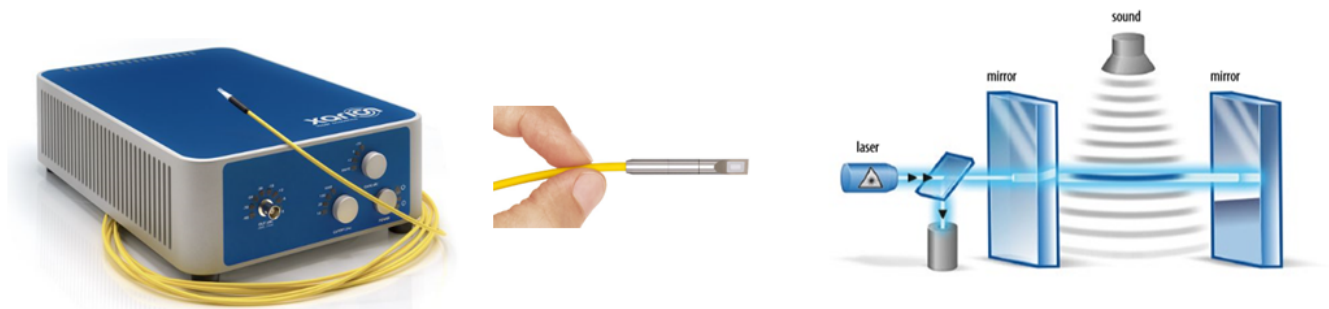


Figure 3. Left: Control unit. Center: Sensor head. Right: Sketch of the setup of the membrane-free optical microphone.

Its detection principle, outlined in Figure 3-right, is described in detail within reference⁴ and relies on the modulation of the refractive index within a medium by sound. Quickly summarized, the refractive index in an isotropic medium, such as air, depends on the polarizability of the medium (a material constant), and density, and therefore on the local acoustic pressure amplitude. This causes small shifts in the wavelength of light such as from a monochromatic laser at wavelength propagating through a sound wave. The wavelength depends on the refractive index as:

$$\lambda(n) = \frac{c}{n(\rho)} \frac{1}{f} = \frac{\lambda_0}{n(\rho)} \quad (1)$$

Here, λ_0 denotes the vacuum wavelength of the laser light, ρ the density and n the refractive index of the medium, c the speed of light in vacuum and f the frequency of the light corresponding to wavelength λ . To detect this modulation of the optical wavelength, a miniaturized Fabry-Pérot cavity consisting of two semi-reflective, rigid mirrors at fixed distance is employed, which constitutes the central element of the detector. The optical intensity of laser light reflected from this cavity follows a transfer function which depends on the detuning of the light with respect to one of the cavity resonances (see Figure 4). Therefore, any change of density caused by the sound field within the Fabry-Pérot cavity causes a change of the reflected light intensity, which can be detected by a

photodiode. This reflected intensity is given by the product of the input intensity I_0 and a transfer function $T_R(q)$, which is given by the Airy function

$$T_R(q) = 1 - \frac{1}{1 + F \sin^2(q/2)} \quad (2)$$

with the finesse coefficient $F = 4R/(1 - R)^2$ and mirror reflectivity R . The round trip phase shift q depends on the laser wavelength $\lambda(n)$ and the mirror distance d as

$$q(n) = \frac{4\pi d}{\lambda(n)} = \frac{4\pi n d}{\lambda_0} \quad (3)$$

As the cavity is rigid, with the mirrors firmly attached to one another at a distance as small as 2 mm, d is constant.

The refractive index of the ambient atmosphere depends on many factors, with temperature and humidity being the most important ones. However, all these factors change very slowly compared to density changes in the form of a sound wave. By locking the laser vacuum wavelength to a working point at the flank of the fringe (dashed black line in Figure 4), slow changes (up to the cut-off frequency of the laser lock) in any parameter are compensated. The interferometer thus acts an "AC measurement" of the refractive index, enabling the detection of sound at arbitrary frequencies.

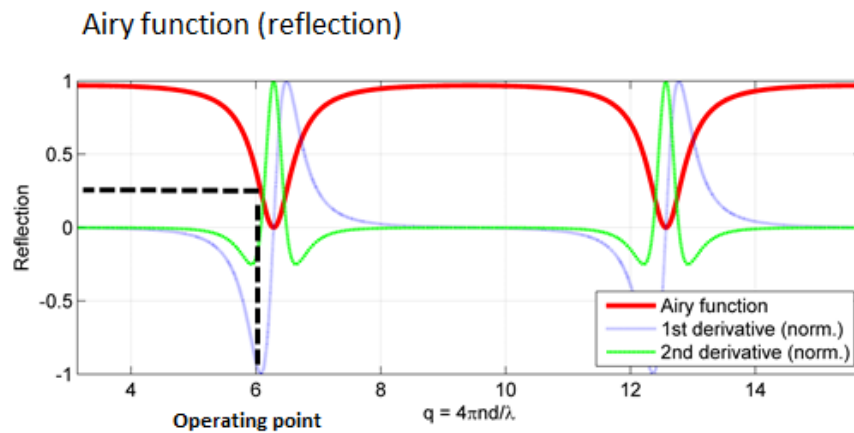


Figure 4. Airy reflection function and derivatives as a function of round-trip phase in the Fabry-Pérot interferometer employed in the optical microphone.

This unique property of the optical microphone is due to the absence of moving parts. Any other detector for airborne (ultra-)sound is limited in frequency by the acceleration and deceleration of a moving mass. For conventional microphones, this limit lies at about 150 kHz, whereas piezoelectric transducers only function in a narrow band range close to their resonance condition. The optical microphone, in contrast, allows the measurement of the full spectrum of sound transmitted through air from 10 Hz to beyond 1 MHz. This is here of high interest to better understand the various mechanisms of sound generation emitted during laser welding processes especially airborne acoustic emissions (AE).

Indeed AE would be due to the displacement of a volumic fraction β of ambient gas of density ρ_0 by hot metallic vapor of density ρ_v ejected from the capillary at a flow rate of $\partial/\partial t(\beta\rho_v)$. The density in a control volume above the keyhole is then

$$\rho = \beta\rho_v + (1 - \beta)\rho_0$$

Farson *et al*⁵ derived the following equation for the pressure field p' under some simplifications and assumptions

$$\frac{1}{c_0^2} \frac{\partial^2}{\partial t^2} p' - \nabla^2 p' = \rho_0 \frac{\partial^2}{\partial t^2} \beta \quad (4)$$

where c_0 is the speed of sound in the ambient gas. This is a common non homogeneous wave equation for the propagation of sound pressure initiated by mass injection. It worth noting that, following this formula, a continuous mass injection does not produce sound.

To conduct inline ultrasound analysis, the analog output of the XARION sensor is sampled by a QASS Optimizer4D system from QASS GmbH. This is a measuring computer that performs real-time Fast Fourier Transform of the signal using a 24bit A/D converter and a maximum sampling rate of 4 MHz.

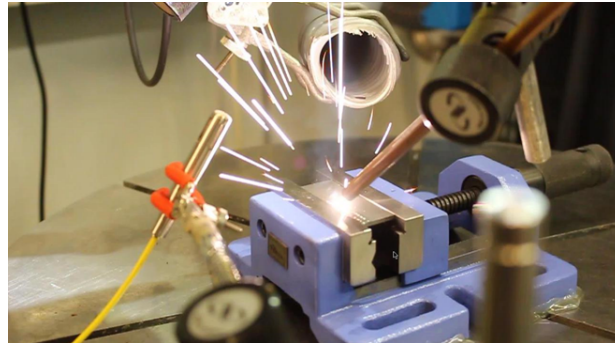


Figure 5. Typical bead on plate configuration showing the microphone sensor head in its protection housing.

3. COUPLED INSTRUMENTED EXPERIMENTS

The aim of the first series of experiments was to evaluate the capability of the optical microphone to record the ultrasound acoustic emission generated by the laser-matter interaction on the part and estimate the possible correlation between it and the welding penetration depth. Welding seams are conducted at different laser powers perpendicular to the butt joint of two elementary half-plane sheets (see Figure 5). Two pulsed laser sources are used, a TRUMPF TruPulse62 with a $280 \mu\text{m}$ spotsize (magnification factor of 1.4) and a TRUMPF TruPulse203 with a $600 \mu\text{m}$ spotsize (magnification factor of 1). The optical microphone sensor head is placed in a dedicated protection sleeve to avoid damage from ejected spatter. The distance of the optical microphone to the laser spot on the part is kept constant for each transverse bead (namely 5 to 10 cm depending of the material and laser power range to avoid sound saturation).

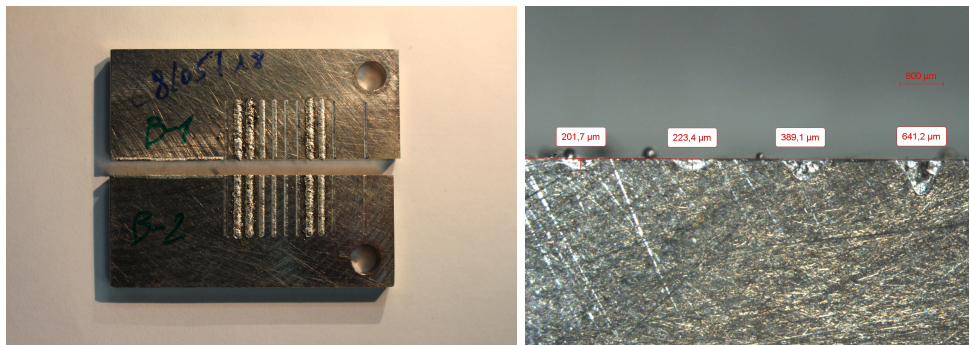


Figure 6. Conduction-limited to keyhole transverse beads on plate experiment and corresponding cross sections.

The second series of experiments aims at analyzing spectrograms and seeking for sound patterns correlated to the OCT measurements. Laser power modulation is applied for each laser pulse in the simple bead-on-plate configuration.

3.1 Conduction limited welding to keyhole welding transition

3.1.1 Stainless steel results

This first experiment is conducted on a welding workplace equipped with a TruPulse62 laser source that has no OCT system. Airborne sounds of the welding are recorded with the optical microphone only and compared to destructive cross section measurements performed later. Figure 7 shows how the sound power evolves with the increasing laser power. The sound level recorded at 800 W laser power is used as a reference. Thanks to the QASS system which calculates and stores an FFT of the signal in real-time, one can also integrate partial sound power in a chosen frequency band. Here the upper ultrasound boundary has been set to 500 kHz after some initial calibration tests. On Figure 7, circles represent the full integration over the sound frequency band from 10 Hz to 500 kHz whereas triangles represent the partial integration from 40 kHz to 500 kHz. The low-frequency of 40 kHz has been chosen here because it is a cut frequency of an internal high passband filter option of the QASS system that will be used in later experiments. Discarding the low-frequency sounds suppresses ambient noise since its spectrum is mostly in the low-frequency audible range. As the absorption of air increases with frequency, high frequency sound sources further away from the process zone are also suppressed through setting this filter.

Sound power integrated over the full frequency band shows a remarkably linear correlation with welding penetration depth. Furthermore, plotting sound level versus laser power, one recognizes in Figure 7 the famous S-curve in which the inflexion point highlights the transition between conduction-limited welding to keyhole welding. In conduction-limited welding mode, the sound power generated by the laser pulse is mostly above the audioacoustic frequencies whereas in keyhole welding mode, up to 60% of the sound power is concentrated in the [0-40 kHz] frequency band.

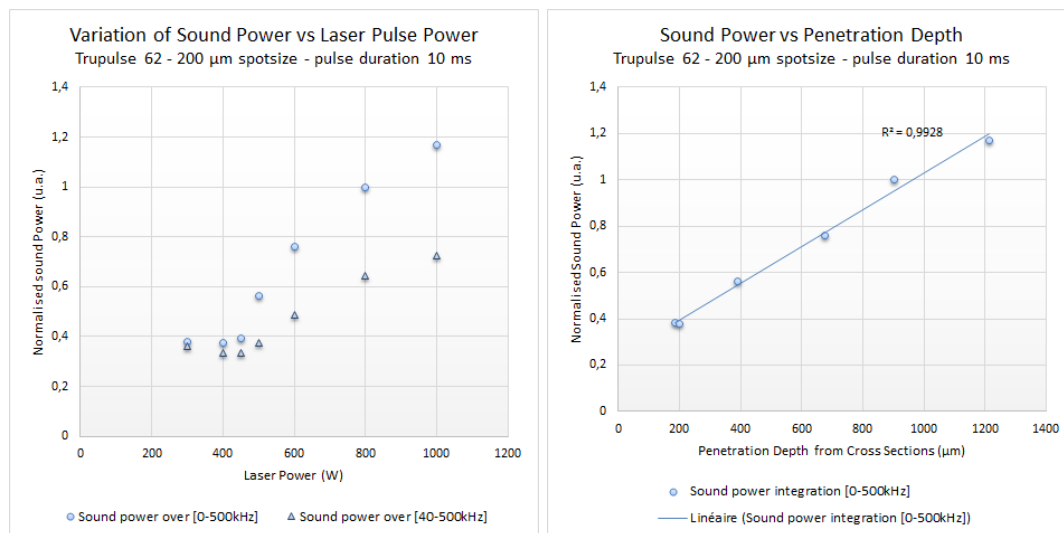


Figure 7. Normalised sound power vs different laser power on TruPulse62. Stainless steel plate. Plate thickness: 2.5 cm. Frequency: 3 Hz, Increment: 0.2 mm, Feed Speed: 0.6 mm. Microphone distance: 5 cm.

Thus, the results compare very well with welder common sense that says that keyhole welding variations can be recognized whereas sound of conduction-limited welding are nearly inaudible. However, even with this direct mapping of sound level to depth, a process control that relies on human-audible range signals is unfavorable. Industrial background noise can be very loud in this frequency region and this was mostly why, in the past, many in-process microphone-based system failed

Because the optical microphone is capable of ultrasound detection, is it self-evident to analyse the sound spectrum for typical signatures or a certain frequency region that could again highlight a linear correlation or a bijection with penetration depth. Figure 8-left shows the sound spectrum recorded during a 800 W pulse. It exhibits several frequency spikes, especially one (in red) that spreads in the band 40 to 90 kHz, centered at

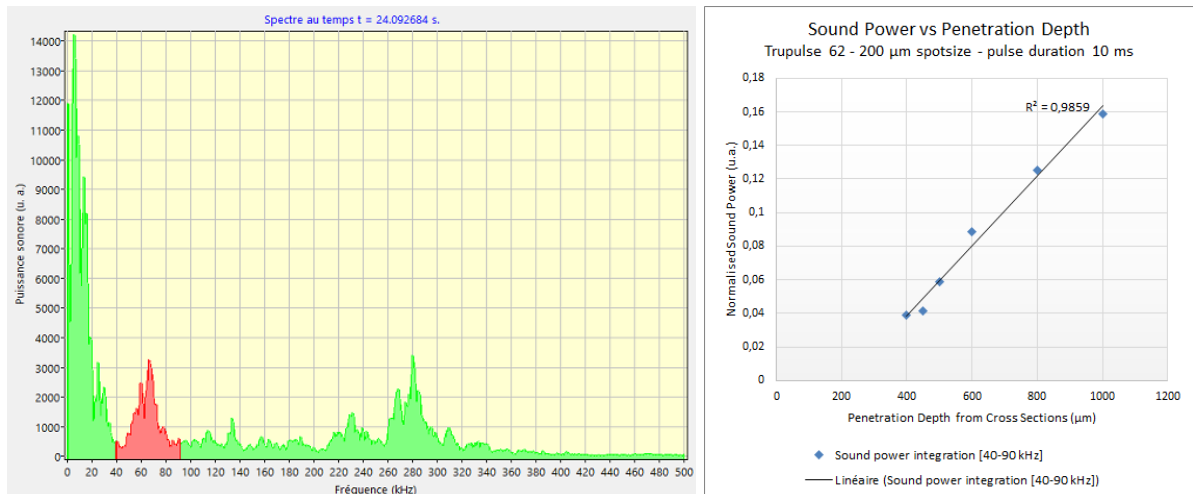


Figure 8. Left: Typical sound spectrum of an 800W-10ms pulse on stainless steel with the TruPulse62 laser source. Right: Correlation between sound power in the [40-90 kHz] frequency band and penetration depth.

70 kHz. The integration of the sound in this band for various laser power gives again the expected result shown on Figure 8-right: a linear correlation between this peak and the penetration depth (a polynomial regression would show a better R^2 coefficient but so far uncertainty of the sound power at those points has not been evaluated and remains subject to further study).

The sound power concentrated in the band [40-90 kHz] represents a few % to 20% of the total sound power. It remains always clearly resolved in the spectra, which leads to a surprisingly effective means of estimating the welding penetration depth. Because it is high above the audio range, it is of special interest in an industrial noisy environment.

3.1.2 TA6V results

The welding workstation connected to the TRUMPF TruPulse203 is equipped with the IDM-instrumented welding laser head. Cross correlations between sound power, OCT and real cross sections are thus possible. The protocol followed is the same as in the previous experiment. Switching to a larger spotsizes implies that the energy density is reduced and likely affects the laser-matter interaction generating a different airborne sound because of a changed vapor ejection regime. The 40 kHz high pass filter has been used for the acquisitions to prevent sound saturation, therefore the audio frequency band is strongly damped, in turn enhancing the upper ultrasound components recorded this time up to 1 MHz. Given sound powers correspond to the integration in the [40-90 kHz] frequency band, where a well-resolved frequency peak remains to exist. Figure 9 shows the comparison between OCT measurements (blue diamond markers), integrated sound power (grey triangles) and metallic cross sections for the various laser power (orange circles). For the sake of the comparison, sound power values are normalised and scaled using the cross section value at 1000 W.

The conduction-limited welding mode spreads, with this configuration, from 0 up to 500 μm of penetration depth, thus no OCT measurement is possible, whereas the ultrasound signal is already present. When the keyhole regime starts, OCT measurements highlight systematic underestimation of approx. 15% to the cross section values. This underestimation is common, if not unavoidable, because firstly, OCT measures keyhole depth and not penetration depth and secondly this effect is re-enforced because of the high reflectivity of titanium which tends to make it difficult to scan properly deep inside the keyhole.

Sound power values as well as OCT values compare overall to cross section values, however they show equally distributed discrepancies of 15%. Figure 10 illustrates that a polynomial correlation exists between ultrasound and depth, demonstrating again the complementary means to the OCT technique through extending the measurement of welding depth also to before the formation of a keyhole.

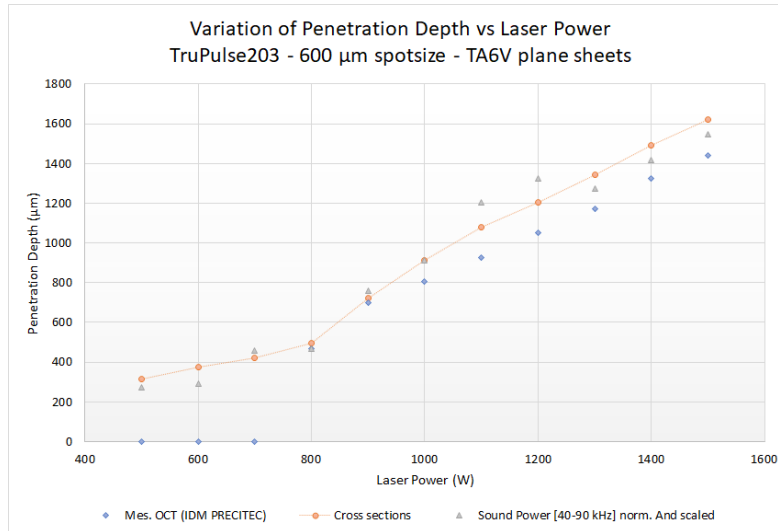


Figure 9. Normalised and scaled sound power vs different laser power on TruPulse203. Titanium TA6V plate. Plate thickness: 2 mm. Frequency: 3 Hz, Increment: 0.2 mm, Feed Speed: 0.6 mm. Microphone distance: 5 cm.

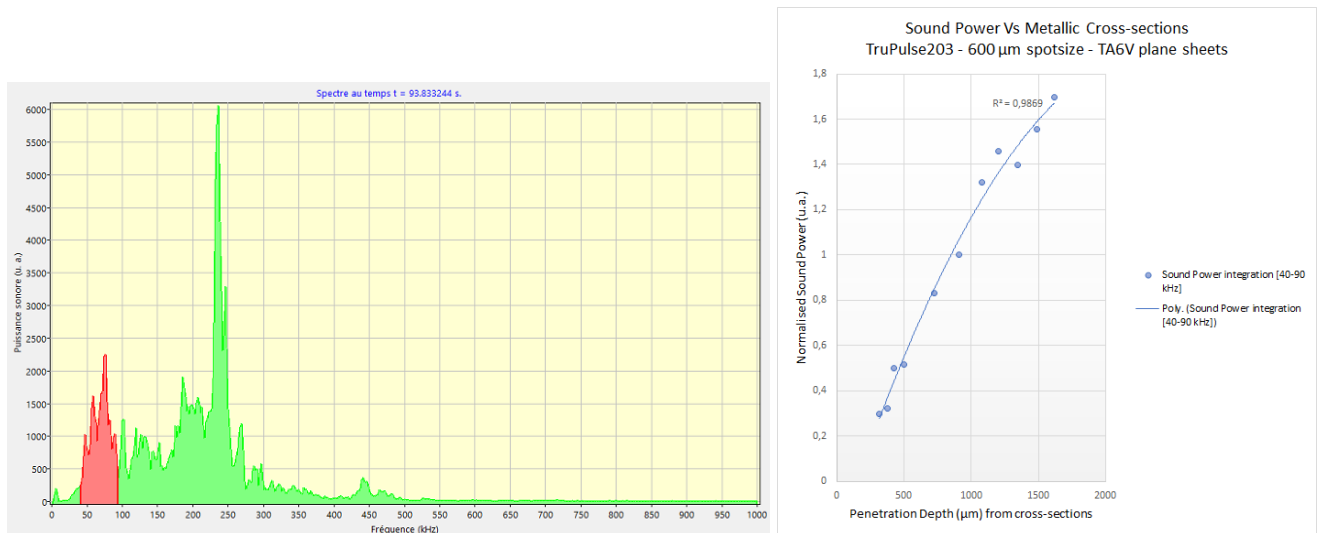


Figure 10. Left: Typical sound spectrum of an 1000 W - 10 ms pulse on TA6V with the TruPulse203 laser source. Right: Correlation between sound power in the [40-90 kHz] frequency band and penetration depth.

3.2 Combined ultrasound and OCT inspections

3.2.1 Power pulse shaping traces in spectrograms

Continuing the experiment of dual use of OCT and airborne ultrasound real-time analysis for in-process control, the next step was to look for a typical ‘fingerprint’ in the sound spectrogram of a single pulse. Indeed varying the power during the pulse duration is a common technique used at the laboratory to reduce, in number and size, porosities in welding beads. Real-time measurements of capillary depth via OCT have been established in the lab as the most efficient way to precisely tune the laser power for controlling the hydrodynamics of the melt pool for each pulse. Thus the metallic vapor exhaust correlated with keyhole variations is expected as being the source of the ultrasound signature.

Figure 11-left shows the keyhole depth variations and the corresponding ultrasound spectrogram of a 20 ms-duration double step power pulse on a 316 stainless steel plate. The capillary depth curve indicates a first expected

digging phase at 1500 W laser power, followed by a prompt drop at the discontinuous step power change, due to partial momentary return of the melt pool inside the cavity. The capillary depth is then maintained at 750 W stable power before shutdown of the laser beam.

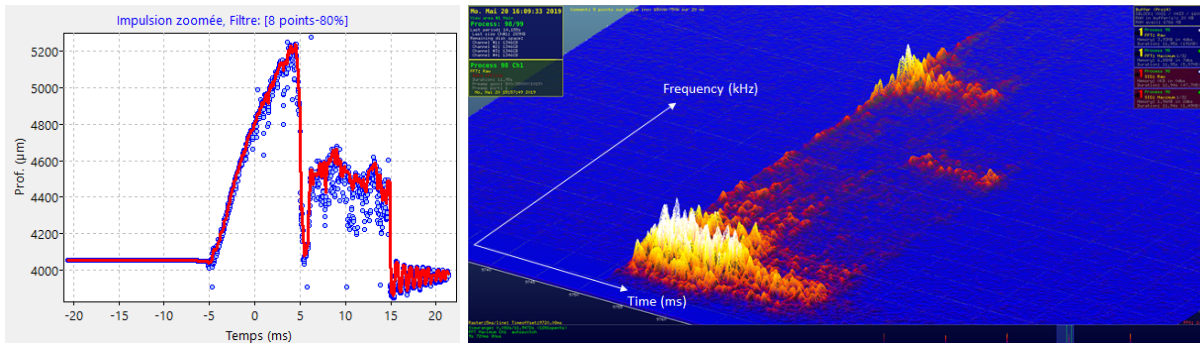


Figure 11. Double step power (1500 W-750 W) 20 ms-duration pulse on 316 stainless steel plate. Left: IDM keyhole depth measurements. Right: Corresponding spectrogram.

While natural in the laser power-time domain, it was surprising to see the laser power steps reproduced in the sound frequency-time domain, as shown in figure 11-right. This is not an obvious transformation since laser power variation in time is a modulation of photons per second whereas sound frequency variation is a time-modulated sound pressure. On the spectrogram, the first upper ultrasound plateau appears at approx. 320 kHz, the second at approx. 230 kHz. Because of its optical transducing principle, it was investigated if the microphone was not also susceptible to wavelength components of the broadband plume light, assuming that the spectrogram could be thus a combination of sound and light. By experimentally masking ultrasound using a glass shield, it was concluded that the spectrogram of the optical microphone was free from light perturbation.

In order to confirm the transform phenomena of laser power ramping into the acoustic frequency-time domain, a double linear ramp pulse power shape was performed. A stable power plateau in between the increasing and decreasing power ramps was included. The duration of the pulse was set to the maximum value available for the laser source, which is 50 ms. As it can be seen in Figure 12, this symmetric start/tail input power results also in a symmetric sound trace spectrally.

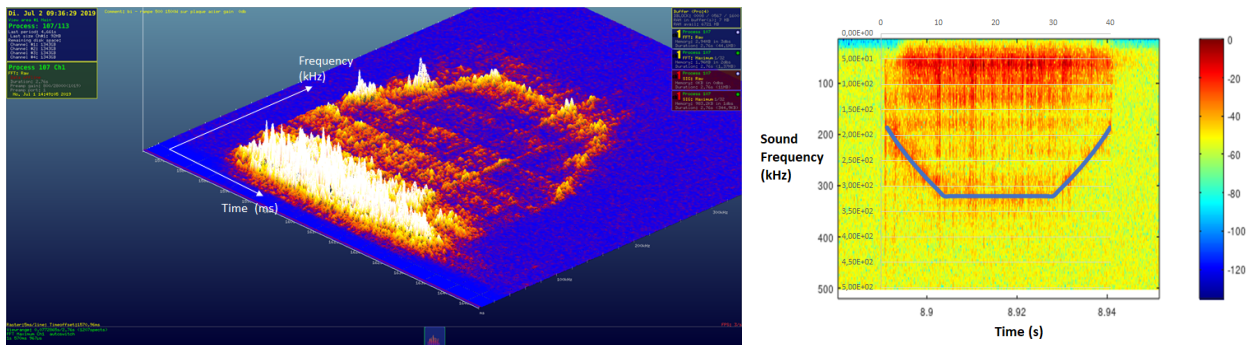


Figure 12. Spectrogram of one laser pulse of 50 ms duration. Start and tail linear ramp [500W-1500W] with 1500W central power plateau experiment. Stainless steel. Left: Real-time spectrogram displayed by the QASS GmbH Optimizer4D analysis software. Right: Spectrogram (GNU octave) with superposed theoretical relaxation oscillation frequency calculation versus laser power using Eq.5.

The question was then, what effect could be the source of this very high frequency sound trace in the spectrogram. Rejecting the idea that it could be originating from some hydrodynamic fluctuations of the melt pool because liquid surface tensions prevent oscillations far above a few kHz, we searched for laser beam oscillations.

Getting back to laser textbooks and reading past articles, we rediscover some previous works⁶⁻⁸ about beam feedback effect on laser cavity and rate equation perturbations. Deviations of the cavity steady state occurs when the pump-light source is switched on, giving rise to well-known relaxation oscillations.^{7,9,10} The dynamic solution of the perturbed cavity rate equations leads to the following formula for the frequency of the relaxation oscillations

$$f = \frac{1}{2\pi} \sqrt{\frac{1 + P/P_{sat}}{\tau_L \tau_p}} \quad (5)$$

where τ_L is excited upper level lifetime, τ_p is the photon lifetime inside the cavity, P_{sat} is the saturated power of the laser cavity and P is the power of the laser cavity. Nd:YAG indicative values⁹ are: $\tau_L = 1.2 \text{ ms}$ and $\tau_p = 1 \text{ } \mu\text{s}$. In equation Eq.5, the P_{sat} parameter is dependent of the geometry of the laser cavity. Thus, using the recommended values of τ_p and τ_L and adjusting P_{sat} to $P_{sat} = 0.320 \text{ W}$, we found a fine match, redrawing the high frequency traces in the resulting spectrograms for all pulse power shaping schemes which were tested (see for example Figure 13).

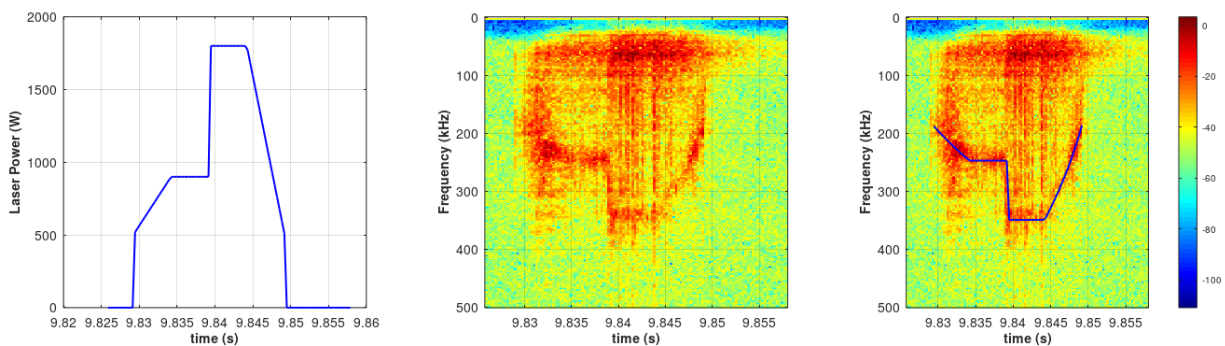


Figure 13. Left: Pulse power shaping scheme. Center: resulting spectrogram of one pulse. Right: Theoretical relaxation oscillation frequency calculation versus laser power using Eq.5 reproduced on the same spectrogram. TruPulse203 laser source. Spotsize: $600 \text{ } \mu\text{m}$. Stainless steel plate.

Even though normally relaxation oscillations should be rapidly damped, in our application, we postulate that because of internal characteristics of the TRUMPF laser source used and the special mode of operation for pulse power shaping, high frequency modulation (even if extremely moderated) remains in the delivered power. In consequence, this gives rise to a tuned-frequency modulation of the laser-matter interaction generating a forced frequency ultrasound source, probably in the plume. It is worth noting that this perturbation effect derives from the feedback of the beam back into the cavity. Even if this trace in the spectrogram could be an interesting feature for an ultrasound fingerprint, it is important to note that changing the laser in use or even the optical configuration (magnification factor or angle) modifies the intensity of the effect. However, the trace in the frequency-time domain is independent of the material welded.

3.2.2 Delayed keyholing experiment

Continuing the inspection of the spectrograms, we noticed, as on Figure 13, that keyhole existence was signaled by strong ultrasound peaks in the [40-120 kHz] frequency region, especially in this case around 64 kHz.

Then a comparable exercise has been conducted with a tantalum plate to delay/separate the creation of the keyhole more clearly and synchronize with the OCT measurements for identification. This material has a very high fusion and vaporization temperature which demands a substantial amount of energy to be deposited into it. In addition we defocused the optical configuration by 4 mm above the plate in order to decrease most of the power density and used a long duration of 40 ms for the pulses. Figure 14 illustrates the keyhole depth curve recorded by OCT (above) in combination with the sound spectrogram from the real-time optical microphone acquisition (below) synchronized on the same timeline. The power steps are respectively 500, 1000, 1500 and 3000 W and have a duration of 10 ms each. On the figure, the dotted vertical lines separate the power steps. When the laser starts and during the first 30 ms, the decreasing depth is interpreted as the growth of the melt

pool. At each step, a corresponding relaxation oscillation frequency rings with an increasing intensity. Finally, at the beginning of the fourth step power of 3000 W, the power density is high enough to immediately open the keyhole, digging very quickly into the matter. Synchronized with the OCT measurements, strong ultrasound signature appears in the [40-120 kHz] frequency region peaked especially about 60 kHz.

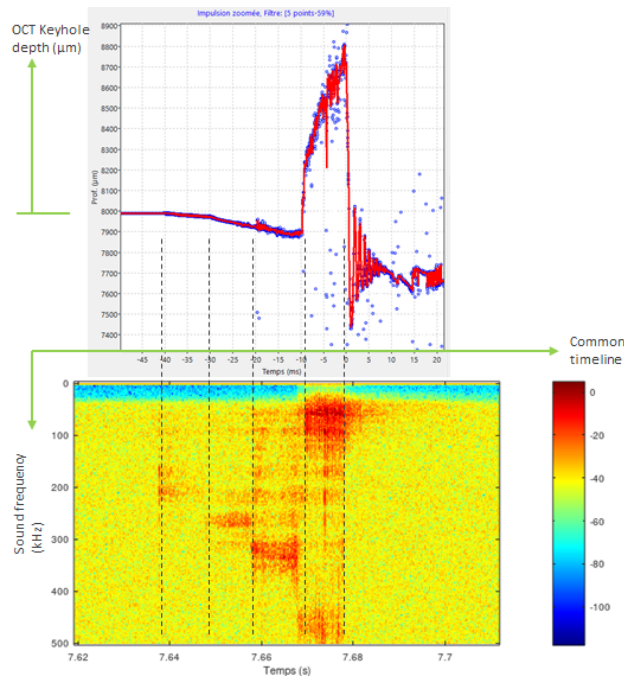


Figure 14. Defocused four plateau power experiment on tantalum plate. Synchronized OCT depth measurements and spectrogram. Delayed keyhole formation until fourth power level reached.

Then, by no doubt, keyhole existence, either on stainless steel, titanium or tantalum plate is signaled by a dense sound peak forest centered at an apparently material-independent 60 kHz frequency line. No theoretical explanation of this effect has been found so far.

4. CONCLUSION

Combination of Optical Coherence Tomography measurements with airborne ultrasound data acquisitions has been demonstrated in this work. Correlation of ultrasound power and welding penetration depth is derived from experimental measurements on different material such as stainless steel or titanium. The integrated sound power in the [40-90 kHz] frequency region, far above the audioacoustic range, allows real operational use of an optical microphone in a loud industrial environment. Accuracy of sound power-derived welding depth estimations compare well with OCT keyhole depth measurements (eg. 15% around bead cross sections). Spectrograms of pulse power shaping exhibit a surprising spectral trace in the frequency-time domain that is explained as the sound emission of a forced frequency tuned laser-matter interaction due to a laser cavity optical feedback effect. Ultrasound ringing frequencies related to the keyhole opening have also been demonstrated with the help of synchronized sound and OCT measurements. While this research remains at its beginning, the combination of OCT with an air-coupled ultrasound optical microphone shows a promising match for the setup of future inline control process of laser welding.

REFERENCES

- [1] Sun, A., Kannatey-Asibu, E., and Gartner, M., "Sensor systems for real-time monitoring of laser weld quality," *Journal of Laser Applications* **11**, 153 (1999).

- [2] Bautze, T. and Kogel-Hollacher, M., “Keyhole depth is just a distance,” *Laser Technik Journal* **4**, 39–43 (2014).
- [3] Authier, N., Baptiste, A., Touvrey, C., Bruyère, V., and Namy, P., “Implementation of an interferometric sensor for measuring the depth of a capillary laser welding,” *ICALEO Proc.* , 904 (2016).
- [4] Fischer, B., Rohringer, W., Panzer, N., and Hecker, S., “Acoustic process control for laser material processing,” *Laser Technik Journal* **5**, 21–25 (2017).
- [5] Farson, D. F. and Kim, K. R., “Generation of optical and acoustic emissions in laser weld plumes,” *Journal of Applied Physics* **85**, 1329 (1999).
- [6] Steen, W. and Mazumder, J., [*Laser Material Processing*], Springer, London (2010 (4th edition)).
- [7] Weerasinghe, V., Kamalu, J., Hibberd, R., and Steen, W., “Acoustic signals from laser back reflection,” *Optics and Laser Technology* **22**, 381–386 (1990).
- [8] Li, L., “A comparative study of ultrasound emission characteristics in laser processing,” *Applied Surface Science* **186**, 604–610 (2002).
- [9] Kärtner, F., “Laser dynamics.” MIT Open CourseWare, 2005 <https://ocw.mit.edu/courses/electrical-engineering-and-computer-science/6-977-ultrafast-optics-spring-2005/lecture-notes/chapter4.pdf>. (Accessed: 11 January 2020).
- [10] Paschotta, R., “Relaxation oscillations.” RP Photonics Encyclopedia, 11 January 2020 https://www.rp-photonics.com/relaxation_oscillations.html. (Accessed: 11 January 2020).